Proton spectra from 800 MeV protons on selected nuclides

R. E. Chrien, T. J. Krieger, R. J. Sutter, M. May, and H. Palevsky
Brookhaven National Laboratory, Upton, New York 11973

R. L. Stearns
Vassar College, Poughkeepsie, New York 12601

T. Kozlowski
Los Alamos Scientific Laboratory, Los Alamos, New Mexico 87545

T. Bauer
University of California, Los Angeles, California 90024

(Received 17 September 1979)

The emission of protons from targets of ^{6}Li, Li, ^{12}C, ^{27}Al, ^{40}Ca, ^{51}V, ^{90}Zr, and Pb under bombardment from 800 MeV protons has been studied using a high resolution proton spectrometer. Spectra were measured at laboratory scattering angles of 5°, 7°, 9°, 11°, 13°, 15°, 20°, 25°, and 30° with special emphasis on the quasifree region. Outgoing momenta corresponding to the region of pion production were examined at 11° and 15°. Absolute cross sections have been derived by reference to known (p,p) scattering data at 800 MeV. The quasifree scattering has been compared to a distorted-wave impulse approximation analysis by summing over the unobserved (struck) nucleon. The systematics of proton production and the applicability of the distorted-wave impulse approximation analyses are discussed.

[NUCLEAR REACTIONS (p,p') on ^{6}Li, Li, ^{12}C, ^{27}Al, ^{40}Ca, ^{51}V, ^{90}Zr, Pb; E_p = 800 MeV, θ_L = 5° to 30°; quasielastic scattering, DWIA analysis.]

I. INTRODUCTION

The elementary aspects of nuclear reactions at high energies were first pointed out by Serber.[1] At high energies, high-momentum transfers to the nucleus occur and the cross section is no longer dominated by coherent effects, but is more affected by the individual nucleon-nucleon interactions. We would thus expect that nucleon-nucleus collision at high energies can be treated as a series of nucleon-nucleon collisions, as suggested by Goldberger[2]; in many cases only one such collision takes place and the interacting nucleons may leave the nucleus without further collisions. Such a collision is called "quasielastic" and the process has been previously studied in a number of experiments.[3] If the scattering process is sufficiently inelastic, mesons can be produced. In the spirit of the two-body interaction philosophy outlined above, we might expect that this deep inelastic process should be dominated by the (3, 3) pion-nucleon resonance.[4] This resonance can also be described as the formation of a "Δ" isobar.

We can illustrate these aspects of the nucleon-nucleus scattering process by reference to Fig. 1, which is a typical cross section curve based on the data of the present experiment, for the case of ^{12}C (p,p') at a laboratory scattering angle of 11°. In the elastic and near elastic region (A) one finds the ground state and various excited states of the recoiling ^{12}C system. These states are not of primary interest in our experiment and will not be further discussed here. In the momentum region corresponding to the free nucleon-nucleon scattering kinematics (B), one sees a broad peak which evidently related to nucleon-nucleon scattering in the nuclear interior. The width of the peak

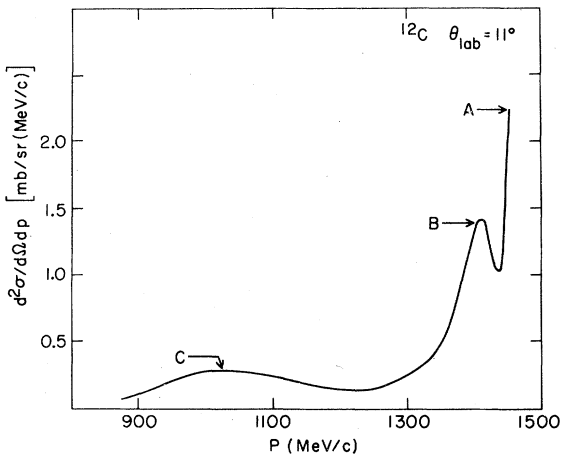

FIG. 1. The smoothed double-differential cross section curve for protons from ^{12}C at a laboratory scattering angle of 11°. The quasielastic and delta-isobar peaks can be seen at momenta near 1410 and 1020 MeV/c, respectively. The elastic scattering and scattering to discrete states of ^{12}C are not shown.

can be attributed to the internal momentum distribution, or Fermi motion, of the nucleons.

At still lower momenta for the outgoing proton, one arrives at a region (C) where meson production is energetically possible. In this region the nucleon-nucleon cross section is dominated by the delta isobar, and we therefore expect to see the effect of that resonance in the proton spectra from the nucleus.

It should be evident from these qualitative considerations that inelastic proton scattering can excite a variety of nuclear processes and this offers a technique for probing gross nuclear features. In the present work a variety of targets have been subjected to 800 MeV protons and the spectra of emerging protons have been examined. The angle and momentum differential cross sections have been determined. The systematic behavior of the gross features of these spectra with target mass and scattering angle are described and the quasielastic region of the spectra are interpreted within the framework of a distorted-wave impulse approximation (DWIA) calculation.

A number of previous experiments on the inclusive proton reactions are described in the literature, although none cover as broad a range of targets and momenta as those described here. They may be found in Refs. 5–11. Much of the DWIA theory has been developed to interpret the more restrictive $(p,2p)$ reaction as first investigated by Tyrén, Maris, and Hillman.[12] [In Ref. 10, the first $(p,2p)$ experimental measurement was attributed to Chamberlain, but this work apparently remains unpublished.] In that analysis the restriction is made that both struck and incoming nucleons leave the nuclear volume and are detected in coincidence. While the coincidence restriction is capable of yielding more definite information about nuclear structure, such as shell effects, the inclusive reaction, or singles measurements, can cover a broader range of possible excitation processes. To present the systematic behavior of the inclusive reaction is the goal of the present work.

II. DESCRIPTION OF EXPERIMENT

The measurements were performed at the Los Alamos Clinton P. Anderson Meson Physics Facility (LAMPF) using the High Resolution Proton Spectrometer (HRS).[13] HRS is a quadrupole-dipole-dipole (QDD) momentum-loss spectrometer with a horizontal scattering plane and a vertical dispersion plane. The 800 MeV proton beam (nominal value—actually 795 MeV) was derived from stripping the accelerated H^--ion beam, with typical beam currents of 0.25 to 10 nA on the target.

HRS operated at an effective resolution $\Delta p/p$ of 2×10^{-4}, a momentum bite of ±1.1%, and a solid angle of ~2 msr. The resolution was limited by the presence of Mylar vacuum windows at the scattering chamber exit and the entrance aperture of the spectrometer. However, for the purpose of this experiment, the resolution was quite adequate.

Detection was accomplished by a set of 5 scintillation detectors and 4 multiwire proportional counters with delay line readouts. These detectors were mounted near the spectrometer focal surface as indicated in Fig. 2. The specifications for these detectors may be found in Table I. The multiwire counters had spatial resolution (σ) of about 0.3 mm and were used to determine particle trajectories in the region of the focal surface. Pulse height and time-of-flight information was derived from the scintillators and used for particle identification, particularly against the large deuteron component present in the spectrometer. Veto counters V_1 and V_2, to define precisely the spectromenter acceptance and to discriminate against pole-face scattering, were arranged as shown in Fig. 2.

Targets of ^{6}Li, Li, ^{9}Be, ^{12}C, ^{27}Al, ^{40}Ca, ^{51}V, ^{90}Zr, and Pb were run at angles of 5°, 7°, 9°, 11°, 13°, 15°, 20°, 25°, and 30°. (For the case of ^{9}Be only a limited momentum range was covered. The primary goal of these runs was to identify α-like nuclear clusters by looking for peaks in the excitation energy spectrum, corresponding kinematically to scattering from particles of mass $A=4$. This topic will be covered in a separate publication.) Only the data for angles larger than 9° have been processed. Calibration targets of deuterated

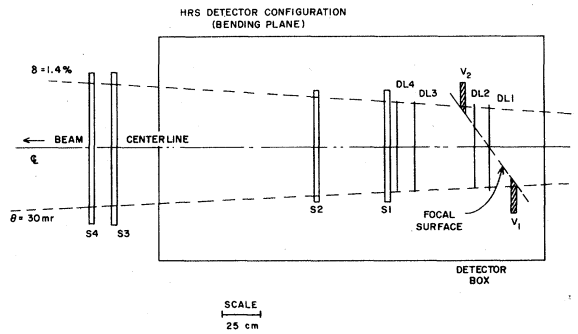

FIG. 2. The detector configuration for this experiment. The counters labeled "*DL*" are multiwire proportional counters with delay line readout. The counters labeled "*V*" are veto scintillators to define the spectrometer aperture. The scintillators labeled "*S*" are used for particle identification through time-of-flight and energy loss measurements. The angular and momentum apertures in the bending plane are shown.

TABLE I. Dimensions for the multiwire proportional counters and the scintillation detectors used in this experiment.

HRS detector specifications		
*V*1	12.70×17.78 ×0.3175 cm	Pilot B
*V*2	12.70×17.78 ×0.3175 cm	Pilot B
*S*1	76.2 × 8.89 ×0.6350 cm	Pilot B
*S*2	77.47×10.795×0.6350 cm	Pilot F
*S*3	106.68×13.97 ×0.9525 cm	NE110
*S*4	106.68×13.97 ×0.9525 cm	NE110
*DL*1 *X*,	58 cm, 1 mm spacings (cathode)	
Y,	11 cm, 3 mm spacings (anode)	
*DL*2[a] *X*,	58 cm, 4 mm spacings (anode)	
*DL*3 *X*,	58 cm, 1 mm spacings (cathode)	
Y,	11 cm, 3 mm spacings (anode)	
*DL*4[a] Same as *DL*2		

[a] These chambers are calibration chambers.

polyethylene and polyethylene were run at all angles. For cross section normalizations, we made use of the (p,p) differential cross sections measured by Willard *et al.*[14] Table II lists in detail the target parameters and the angle and momentum ranges covered. Not all targets were investigated in the momentum region corresponding to delta-isobar production, although the quasi-elastic region was investigated for all.

The targets, which range typically from 10 to 50 mg/cm^2 were 4.5×10 cm in size and were mounted on a remotely actuated target wheel located in the scattering chamber.

Several beam monitors were simultaneously available. Two Ar-Co_2-ion chambers at 50 mm pressure were located inside the scattering chamber 1 m behind the target, and a third was placed about 10 m downstream. The ion chambers saturated at the higher currents used. To cover the higher current region a secondary emission monitor (SEM) with a gain of 0.4 was placed 4 m down-

TABLE II. A summary of the target parameters and the momentum ranges covered in this experiment.

Target	Thickness mg/cm^2	Angles°	Momentum range MeV/*c*	Target	Thickness mg/cm^2	Angles°	Momentum range MeV/*c*
^{6}Li*	48.81	11	1450→ 880		48.44	25	1447→1066
	48.81	13	1452→1230		48.44	30°	1452→ 907
	48.81	15	1460→ 725	^{51}V	18.92	11	1450→ 880
	48.81	20	1440→1070		18.92	13	1452→1230
	48.81	25	1450→ 947		18.92	15	1460→1160
	48.81	30°	1400→ 907		18.92	20	1455→1070
Li*	54.378	11	1450→ 880		18.92	25	1447→1035
	54.378	13	1452→1230		18.92	30	1452→ 907
	54.378	15	1460→1180	^{90}Zr	49.82	11	1450→1230
	54.378	20	1440→1070		49.82	13	1452→1230
	54.378	25	1450→ 946		49.82	15	1460→ 725
	54.378	30°	1402→ 905		49.82	20	1455→1070
^{12}C	40.83	11	1450→ 880		49.82	25	1426→1035
	40.83	13	1452→1230		49.82	30	1452→ 906
	40.83	15	1460→ 725	^{208}Pb	54.907	11	1450→1230
	40.83	20	1440→1070		54.907	13	1452→1230
	40.83	25	1450→ 946		54.907	15	1460→ 725
	40.83	30°	1438→ 907		54.907	20	1428→1070
^{27}Al	57.58	11	1450→ 880		54.907	25	1447→1034
	57.58	13	1452→1230		54.907	30	1452→ 907
	57.58	15	1460→ 725	$^1_1$H	43.78 (CH_2)	15°	1355→ 730
	57.58	20	1440→1070	$^2_1$H	19.6 (CD_2)	15°	1300→ 730
	57.58	25	1452→ 946				
	57.58	30°	1401→ 906	^{9}Be	46.2	15°	1454→1377
^{40}Ca	48.44	11	1450→1230		46.2	20	1443→1317
	48.44	13	1452→1230		46.2	25	1414→1300
	48.44	15	1460→ 725		46.2	30	1428→1140
	48.44	20	1455→1070				

stream of the target. In addition a pair of scintillator counter telescopes viewed the beam-target interaction region at 45° and 120°. These were useful for monitoring beam steering and phase space. An additional monitor which was used occasionally was a thin CH_2 foil in the beam upstream of the scattering chamber and viewed by two counter telescopes to the left and right of the beam. The redundant beam monitors were very useful for readily identifying malfunctioning instruments and bad beam conditions. The configuration of monitors within and near the scattering chamber is drawn in Fig. 3.

The HRS spectrometer is used with the horizontal plane containing the principal component of scattering angle and a vertical plane containing the bending or dispersion direction. The data from events detected by the multiwire counters were used to define the particle trajectories and compute their intersections with the spectrometer focal surface, from which both momentum difference $\delta(P_0 - P)/P$ and scattering angle θ could be determined.

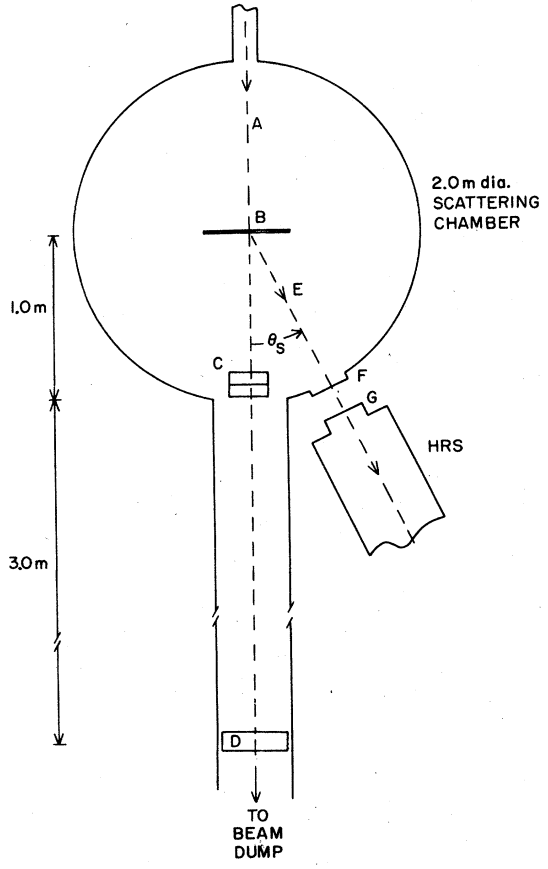

FIG. 3. The arrangement of beam monitors near the target wheel in the scattering chamber. The incident beam, shown at "*A*", intersects the target wheel "*B*" and traverses ion chambers "*C*" (2 chambers) and "*D*". The scattered beam "*E*" leaves the scattering chamber at "*F*" and enters the spectrometer at "*G*".

The momentum region was covered by a series of runs with $\delta = \pm 1.1\%$ from the elastic region to well below the quasielastic. An angular range of ±1° was covered by the focal plane. At each angle calibration runs were taken with polyethylene and deuterated polyethylene foils at momenta near the (p,p) and (p,d) elastic scattering points. To record the data, we used the standard HRS data acquisition system based on the PDP-11/45.

In general, event rates in the order of 100 per sec were recorded on magnetic tape, with about 85 000 events for each spectrometer momentum and angle setting. About 1500 runs were taken in all, 3 runs per 730 m reel of tape. Later the tapes were scanned to produce a matrix of 461 ×20 channels as a function of δ and θ, respectively, on the focal plane. An example of the data, binned in increments of $\delta = (P_0 - P)/P$ of 7×10^{-4} and $\Delta\theta = 0.093\,75°$ is shown in Fig. 4. This figure shows a portion of the focal plane binned in the above size channels for a deuterated polyethylene scatterer. The shaded portion indicates the region of the (δ, θ) scattering plane containing protons elastically scattered from deuterium. Spectra were produced from data similar to those of Fig. 4; for example, a momentum spectrum could be produced from a cut holding θ constant, or alternatively a "missing mass" or excitation energy spectrum could be produced by integrating along the trajectory defined in the (δ, θ) plane by a 2-body relativistic kinematics relationship. Separate runs corresponding to different momentum (δ) regions were joined together and the trajectories integrated across the boundary region.

The double-differential cross section $d^2\sigma/d\Omega dp$ determined in this experiment are averaged over the spectrometer angular acceptance of 2°. In principle this procedure would lead to the additional broadening of the quasielastic peak, since the peak position follows the kinematics for (p,p) scattering, which defines a relationship between scattering angle and momentum. However, the kinematic variation of (p,p) scattering over ±1° centered at 15° is 22.6 MeV/c and at 30° is 36.2 MeV/c. The natural linewidth due to Fermi motion is ~100 MeV/c. Thus no significant distortion of the data is introduced by this averaging. The inherently high resolution of the HRS is not needed for the smoothly varying cross sections characteristic of quasielastic scattering or delta-isobar production. The high resolution is, however, essential in identifying and correcting for the usually troublesome problem of hydrogen contamination of the target surfaces. For the ^{6}Li, ^{12}C, ^{40}Ca, and Pb samples, some surface hydrogen

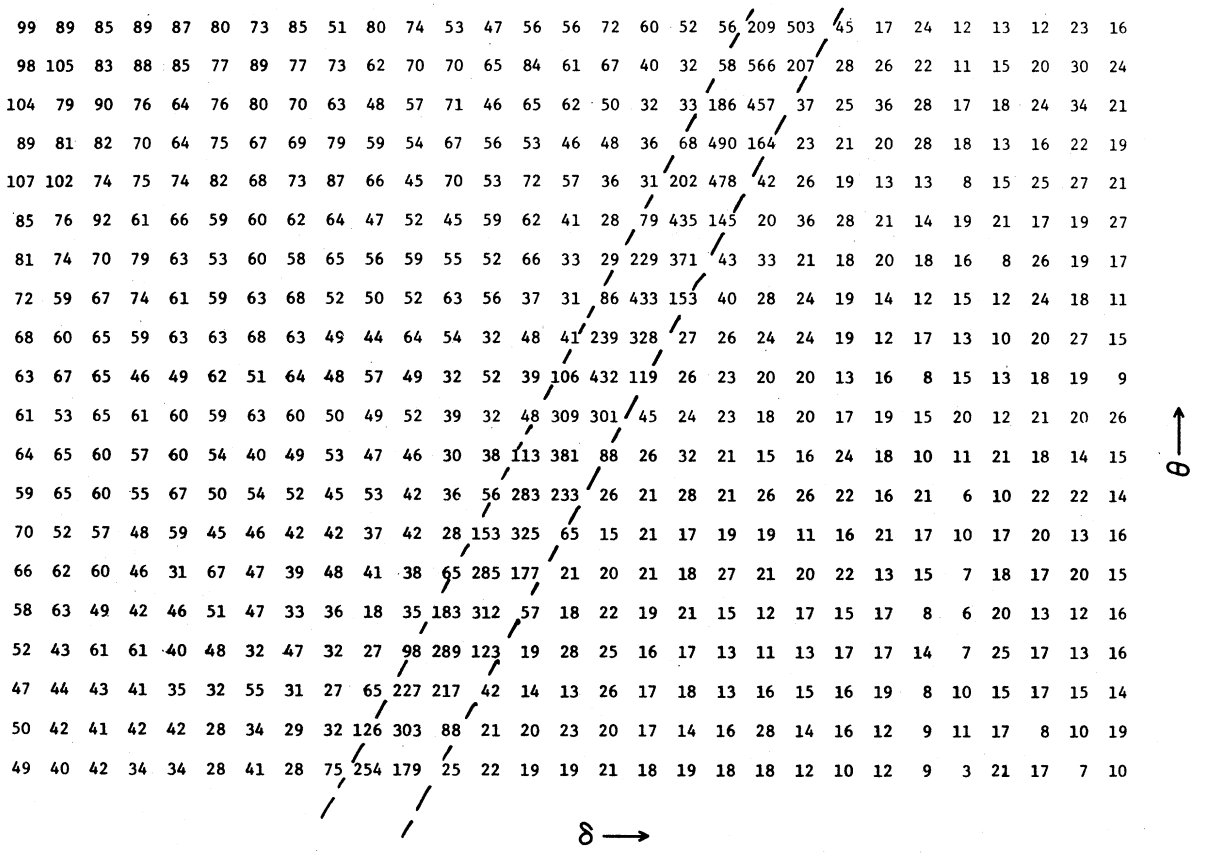

FIG. 4. A portion of the data across the focal plane and binned as indicated in the text. The dotted lines highlight the trajectory obtained from elastic scattering of protons from deuterium. All the data of this experiment were analyzed by first binning the digital output of the delay line chambers in the δ (bending) and θ planes and performing calculations on the binned data.

contamination, probably from water, is evident. Figure 5 shows a plot of the quasielastic region in ^{12}C. The hydrogen contamination shows up as a pronounced narrow peak superimposed on the smoothly varying ^{12}C cross section. The sizes of the peak in the various runs indicate contamination at a level of approximately 1000 at. ppm. The resulting incremental cross section is readily identified and subtracted. All of our targets were surveyed in this manner and corrected as necessary.

III. SURVEY OF RESULTS

The results of this experiment are summarized in the form of tables (see Tables III–VIII) of the double-differential cross section $d^2\sigma/d\Omega dp$, mb/[sr (MeV/c)], for the nine targets of the experiment, in steps of about 10 MeV/c. For visualization of the momentum distribution, the 11°, 20°, and 30° laboratory angle spectra are also shown in Figs. 6–8. In addition, Fig. 9 shows the region of the Δ-isobar production, which was examined in detail for ^{1}H, ^{2}H, ^{6}Li, ^{12}C, ^{27}Al, ^{40}Ca, and ^{208}Pb at 15°.

For the elemental targets Li and Pb, the elemental cross sections are shown. The hydrogen and deuterium targets, in the form of polyethylene and deuterated polyethylene have been corrected for carbon content.

Inspection of Figs. 6–9 indicates the general features observed for the (p,p') reaction. The broad quasielastic peak located near the momentum corresponding to free p,p scattering is clearly evident. For the 15° data of Fig. 9 we see also the smaller peak associated with pion production through the 3,3 resonance corresponding to Δ-isobar formation. A distinct minimum separates the two peaks. We see a tendency, in these figures, for the isobar peak to be less pronounced as the mass of the target increases. This tendency may be ascribed to the relatively more important role played by multiple scattering processes as the number of target nucleons increases. Harp *et al.*[15] have obtained reasonable fits for the emitted proton spectra using an intronuclear cascade model[16,17]

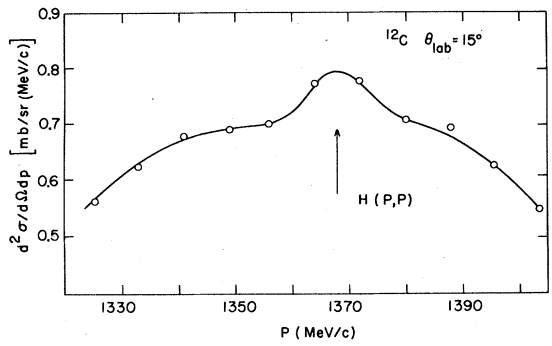

FIG. 5. A portion of the outgoing momentum region for ^{12}C at 15°. Superimposed on the broad quasifree peak is a narrow peak corresponding to elastic scattering from a hydrogen impurity.

in which the Δ isobars are allowed to interact with other nucleons.

The area under the quasielastic peak may be more or less directly related to the number of effective nucleons participating in the quasifree scattering process. The integral under the peak is fairly well defined for angles of 13° and larger and is shown in Fig. 10 as a function of target mass. The cross sections form straight lines on a log-log plot and thus the cross section is well represented by a functional dependence of the form $\sigma = \sigma_0(A)^n$, where n is approximately 0.4. Also shown on the plot is the (p,p) cross section on hydrogen, plotted for $A=1$. This point lies quite close to the straight line. This dependence is close to what may be expected for a purely peripheral scattering process, since the projected

TABLE III. Smoothed cross sections in units of mb/[sr(MeV/c)] for an angle of 11°. These cross sections were obtained by smoothing point by point data obtained in this work. In some cases the interpolation has been performed between nonoverlapping data sets at different momenta.

P (MeV/c)	^{6}Li	Li	^{12}C	^{27}Al	^{40}Ca	^{51}V	^{90}Zr	^{208}Pb
880	0.137	0.162	0.222	0.360		0.600		
900	0.165	0.163	0.235	0.363		0.600		
920	0.180	0.171	0.241	0.378		0.604		
940	0.188	0.179	0.247	0.390		0.608		
960	0.190	0.182	0.253	0.395		0.612		
980	0.190	0.185	0.259	0.399		0.616		
1000	0.188	0.188	0.265	0.400		0.620		
1020	0.184	0.190	0.270	0.405		0.624		
1040	0.190	0.192	0.275	0.400		0.628		
1060	0.190	0.188	0.272	0.395		0.632		
1080	0.180	0.185	0.265	0.390		0.635		
1100	0.168	0.177	0.250	0.380		0.625		
1120	0.153	0.155	0.228	0.350		0.580		
1140	0.138	0.140	0.206	0.328		0.524		
1160	0.119	0.122	0.184	0.306		0.467		
1180	0.100	0.105	0.162	0.283		0.414		
1200	0.083	0.087	0.140	0.260		0.370		
1220	0.065	0.074	0.125	0.239	0.22	0.340	0.350	0.42
1240	0.060	0.068	0.110	0.218	0.22	0.320	0.320	0.44
1260	0.062	0.072	0.115	0.204	0.22	0.330	0.340	0.47
1280	0.065	0.082	0.150	0.190	0.26	0.380	0.380	0.48
1300	0.080	0.112	0.180	0.220	0.330	0.480	0.500	0.62
1320	0.125	0.14	0.260	0.360	0.48	0.620	0.690	0.82
1340	0.195	0.23	0.37	0.630	0.81	0.900	1.010	1.200
1360	0.385	0.540	0.62	0.970	1.22	1.420	1.55	1.75
1380	0.700	0.735	1.041	1.200	1.64	1.900	2.0	2.30
1400	1.025	1.065	1.252	1.660	2.05	2.28	2.500	3.11
1410	1.165	1.197	1.415	1.710	2.20	2.52	2.820	3.40
1415	1.212	1.198	1.430	1.770	2.21	2.57		3.46
1420	1.130	1.130	1.423	1.730	2.18			
1425	1.060	1.100	1.390	1.740	2.17			
1430	1.020	1.325	1.060	1.860				
1435	1.22	1.425	0.940	1.960				
	±6.5 [a]	±6.5	±6.2	±5.9	±6.2	±5.9	±5.9	±6.2

[a] Approximate systematic cross section errors in %.

TABLE IV. Smoothed cross sections in units of mb/[sr(MeV/c)] for an angle of 13°. These cross sections were obtained by smoothing point by point data obtained in this work. In some cases the interpolation has been performed between nonoverlapping data sets at different momenta.

P (MeV/c)	^{6}Li	Li	^{12}C	^{27}Al	^{40}Ca	^{51}V	^{90}Zr	^{208}Pb
1215	0.045	0.050	0.097	0.155	0.19	0.200	0.290	0.34
1225	0.050	0.055	0.100	0.160	0.21	0.215	0.300	0.36
1235	0.055	0.060	0.110	0.175	0.22	0.230	0.310	0.37
1245	0.060	0.068	0.122	0.178	0.23	0.250	0.340	0.40
1255	0.065	0.075	0.136	0.202	0.24	0.270	0.360	0.42
1265	0.070	0.085	0.150	0.225	0.28	0.300	0.400	0.46
1275	0.090	0.100	0.170	0.255	0.30	0.335	0.450	0.53
1285	0.110	0.122	0.205	0.300	0.36	0.385	0.530	0.60
1295	0.140	0.150	0.250	0.355	0.44	0.455	0.620	0.69
1305	0.160	0.188	0.305	0.420	0.520	0.535	0.720	0.81
1315	0.210	0.242	0.379	0.517	0.650	0.640	0.840	0.97
1325	0.280	0.320	0.467	0.636	0.750	0.760	0.970	1.11
1335	0.360	0.410	0.557	0.750	0.870	0.880	1.110	1.28
1345	0.445	0.505	0.645	0.860	1.01	0.995	1.255	1.48
1355	0.550	0.622	0.729	0.966	1.16	1.105	1.430	1.72
1365	0.700	0.775	0.830	1.080	1.31	1.210	1.630	2.01
1375	0.835	0.882	0.912	1.155	1.41	1.335	1.780	2.23
1380	0.870	0.910	0.940	1.175	1.44	1.385	1.850	2.31
1385	0.872	0.912	0.950	1.190	1.48	1.422	1.900	2.37
1390	0.875	0.910	0.952	1.20	1.52	1.455	1.940	2.40
1395	0.865	0.908	0.955	1.20	1.52	1.478	1.970	2.43
1400	0.855	0.890	0.955	1.21	1.54	1.490	1.990	2.44
1405	0.840	0.855	0.952	1.21	1.55	1.510	2.000	2.44
1410	0.820	0.815	0.950	1.20	1.55	1.515	1.990	2.45
1415	0.765	0.790	0.930	1.19	1.52	1.480	1.980	2.40
1420	0.700	0.780	0.840	1.17	1.44	1.442	1.960	2.36
1425	0.685	0.780	0.780	1.14	1.33	1.390	1.940	2.34
1430	0.700	0.790	0.750	1.115		1.480	1.910	2.36
1435	1.00	0.810	0.775	1.090		1.580	1.880	
1440	1.665	1.610	2.04	1.050				
	±6.5 [a]	±6.5	±6.2	±5.9	±6.2	±5.9	±5.9	±6.2

[a] Approximate systematic cross section errors in %.

annular area of the nucleus would vary as $A^{1/3}$. Consequently the quasielastic scattering process is apparently a surface phenomenon.

In general the statistical accuracy of the data, binned in segments of 10 MeV/c for the outgoing proton, is between 1 and 2% over the region of the quasifree peak. The contributions of systematic errors in this experiment are much larger and much more difficult to evaluate. We have attempted to do so on the basis of reproducibility from run to run.

The significant systematic errors arise from several distinct sources.

(1) *Beam monitoring.* An intercomparison of the several beam monitors shows discrepancies attributable to changes in beam quality (phase-space distribution) and beam intensity variations. The redundant monitoring employed and the repetition of supposedly identical runs allow us to assign an error based on observed variations. This amounts to a standard deviation of 2%, after exclusion of obviously malfunctioning monitors in each run.

(2) *Target errors.* These arise from target nonuniformities, errors in thickness determinations, target backing correction, and correction for impurities, such as water. In some cases, specifically the hydrogen and deuteron targets, a correction was applied for the carbon present in the polyethylene material of which the target is composed. Target-thickness errors range from 0.3% to about 2% in the worst cases.

(3) *Corrections for efficiency across the focal plane.* A correction was applied to the data to account for the change in effective aperture, or efficiency from one edge of the focal plane to the other. This correction was measured for ^{12}C elastic scattering. It is very nearly linear over

TABLE V. Smoothed cross sections in units of mb/[sr(MeV/c)] for an angle of 15°. These cross sections were obtained by smoothing point by point data obtained in this work. In some cases the interpolation has been performed between nonoverlapping data sets at different momenta.

P (MeV/c)	^{6}Li	Li	^{12}C	^{27}Al	^{40}Ca	^{51}V	^{90}Zr	Pb	^{2}H	^{1}H
725			0.141	0.219	0.294		0.459	0.605	0.0365	0.0337
730	0.086		0.137	0.22	0.2935				0.0370	0.0340
790	0.090		0.135	0.221	0.293		0.438	0.569	0.0477	0.038
850	0.097		0.146	0.226	0.304		0.430	0.568	0.0565	0.0417
900	0.102		0.148	0.227	0.312		0.435	0.570	0.0610	0.0451
940	0.106		0.154	0.228	0.310		0.430	0.565	0.0640	0.0471
1000	0.105		0.150	0.237	0.305		0.433	0.550	0.0630	0.0478
1050	0.096		0.149	0.229	0.295		0.401	0.502	0.0570	0.0430
1090	0.088		0.138	0.218	0.280		0.360	0.462	0.0485	0.0367
1120	0.078		0.129	0.190	0.263		0.360	0.432	0.0420	0.030
1160	0.067	0.067	0.112	0.181	0.244	0.274	0.360	0.434	0.0280	0.017
1200	0.057	0.066	0.108	0.180	0.250	0.310	0.356	0.436	0.0185	
1220	0.062	0.073	0.115	0.192	0.259	0.365	0.368	0.470	0.0168	
1240	0.070	0.092	0.143	0.235	0.295	0.400	0.400	0.505	0.0160	
1260	0.102	0.130	0.207	0.297	0.337	0.455	0.500	0.630	0.0162	
1280	0.155	0.188	0.278	0.410	0.514	0.57	0.670	0.780	0.0220	
1300	0.234	0.291	0.411	0.560	0.710	0.72	0.890	1.05	0.0300	
1310	0.300	0.359	0.458	0.647	0.817	0.80	1.02	1.21		
1320	0.382	0.441	0.532	0.713	0.925	0.89	1.140	1.36		
1330	0.455	0.506	0.600	0.777	0.960	0.95	1.270	1.50		
1340	0.542	0.624	0.678	0.856	1.106	1.05	1.370	1.71		
1350	0.616	0.619	0.695	0.870	1.12	1.10	1.47	1.81		
1360	0.670	0.700	0.719	0.915	1.255	1.16	1.59	2.01		
1365	0.708	0.745	0.747	0.930	1.26	1.18	1.59	2.08		
1370	0.710	0.721	0.748	0.920	1.262	1.19	1.590	2.16		
1375	0.692	0.714	0.736	0.918	1.245	1.20	1.58	2.12		
1380	0.690	0.680	0.710	0.925	1.23	1.20	1.57	2.08		
1385	0.682	0.685	0.690	0.930	1.22	1.20	1.55	2.06		
1390	0.650	0.661	0.660	0.900	1.21	1.19	1.52	2.05		
1395	0.610	0.577	0.635	0.880	1.12	1.17	1.500	1.97		
1400	0.550	0.539	0.584	0.860	1.05	1.14	1.460	1.89		
1405	0.510	0.500	0.547	0.830	0.995	1.10	1.420	1.85		
1410	0.511	0.441	0.530	0.820	0.986	1.05	1.380	1.82		
1415	0.460	0.447	0.497	0.830	0.869	1.015	1.34	1.77		
1420	0.408	0.400	0.437	0.840	0.853	0.97	1.30	1.73		
1425	0.353	0.403	0.360	0.800	0.848	0.889	1.26	1.68		
1430	0.359	0.356	0.390	0.785	0.844	0.85	1.23	1.604		
1435	0.418	0.310	0.43	0.837	0.797	0.810	1.21	1.545		
1440	0.617	0.890	1.06	0.949	0.750	0.762	1.20	1.46		
	±6.5 [a]	±6.5	±6.2	±5.9	±6.2	±5.9	±5.9	±6.2	±6.6	±6.6

[a] Approximate systematic cross section errors in %.

the focal plane and amounted to ±8%, referred to the center. We allow a 1% error component due to this effect.

(4) *Nonlinearity corrections.* The nonlinearity of the delay line readout multiwire proportional counters was inferred from a set of calibration chambers with accurately known wire spacings. The nonlinearity correction was fitted to a second degree polynomial; the maximum deviation from linearity amounts to ±10% over the focal plane. The error introduced by this correction was considered less than 0.1% and thus negligible.

(5) *Momentum errors.* These arise in setting the spectrometer magnetic fields when piecing together a spectrum comprised of the many individual runs, each reflecting the narrow momentum bite of the spectrometer. We estimate the resulting momentum uncertainty as about 1 MeV/c, which has a negligible influence on cross sections.

(6) *Reference standard errors.* The authors ascribe an error of between 2.3% and 5% to the (p,p) standard data of Ref. 14.

TABLE VI. Smoothed cross sections in units of mb/[sr(MeV/c)] for an angle of 20°. These cross sections were obtained by smoothing point by point data obtained in this work. In some cases the interpolation has been performed between nonoverlapping data sets at different momenta.

P (MeV/c)	^{6}Li	Li	^{12}C	^{27}Al	^{40}Ca	^{51}V	^{90}Zr	Pb
1070	0.0575	0.0600	0.103	0.1675	0.205	0.2100	0.2950	0.360
1080	0.0560	0.0625	0.105	0.1700	0.207	0.2225	0.2975	0.365
1090	0.0550	0.0600	0.108	0.1725	0.208	0.2250	0.2988	0.360
1100	0.0565	0.0613	0.110	0.1750	0.210	0.2300	0.3000	0.368
1110	0.0580	0.0625	0.113	0.1775	0.211	0.2320	0.3050	0.380
1120	0.0563	0.0638	0.115	0.1825	0.214	0.2400	0.3100	0.390
1130	0.0610	0.0663	0.121	0.1900	0.220	0.2450	0.3150	0.400
1140	0.0615	0.0688	0.124	0.1975	0.230	0.2550	0.3250	0.410
1150	0.0688	0.0738	0.129	0.2100	0.240	0.2625	0.3375	0.420
1160	0.0713	0.0800	0.138	0.2175	0.255	0.2700	0.3500	0.428
1170	0.0825	0.0900	0.150	0.2375	0.270	0.2850	0.3725	0.438
1180	0.0938	0.1050	0.170	0.2525	0.290	0.3200	0.4000	0.460
1190	0.1063	0.1200	0.190	0.2850	0.310	0.3275	0.4250	0.488
1200	0.1213	0.1400	0.208	0.3050	0.330	0.3525	0.4550	0.523
1210	0.1463	0.1625	0.228	0.3325	0.355	0.3800	0.4925	0.565
1220	0.1700	0.1900	0.254	0.3600	0.400	0.4100	0.5250	0.620
1230	0.1888	0.2075	0.285	0.3850	0.430	0.4400	0.5500	0.675
1240	0.2200	0.2413	0.313	0.4125	0.470	0.4725	0.6100	0.743
1250	0.2525	0.2800	0.338	0.4400	0.513	0.5025	0.6588	0.798
1260	0.2875	0.3175	0.355	0.4600	0.550	0.5300	0.7050	0.860
1270	0.3238	0.3400	0.380	0.4875	0.590	0.5625	0.7575	0.930
1280	0.3500	0.3650	0.390	0.5150	0.615	0.5950	0.8150	0.990
1290	0.3700	0.3800	0.398	0.5300	0.640	0.6175	0.8550	1.045
1300	0.3838	0.3825	0.403	0.5450	0.645	0.6250	0.8700	1.080
1310	0.3788	0.3750	0.403	0.5538	0.650	0.6275	0.8750	1.105
1320	0.3513	0.3550	0.395	0.5500	0.638	0.6200	0.8300	1.108
1330	0.3250	0.3300	0.385	0.5400	0.610	0.5975	0.8355	1.090
1340	0.2700	0.3000	0.345	0.5100	0.575	0.5563	0.8038	1.053
1350	0.2225	0.2525	0.308	0.4700	0.535	0.5475	0.7550	1.005
1360	0.1850	0.2050	0.265	0.4288	0.485	0.4825	0.7025	0.994
1370	0.1463	0.1625	0.228	0.3850	0.425	0.4375	0.6275	0.830
1380	0.1150	0.1150	0.191	0.3350	0.368	0.4100	0.5600	0.798
1390	0.0800	0.0850	0.148	0.2750	0.300	0.3250	0.4950	0.695
1400	0.0538	0.0625	0.120	0.2250	0.260	0.2975	0.4400	0.605
1410	0.0438		0.108	0.1900	0.215	0.2775	0.3925	0.550
1420			0.073	0.1550	0.170	0.1975	0.3200	0.440
1430				0.1300	0.140	0.1650	0.1325	0.380
1440				0.1050		0.1275		
1450								
	±6.2 [a]	±6.2	±5.8	±5.5	±5.8	±5.5	±5.5	±5.8

[a] Approximate systematic cross section errors in %.

IV. DWIA ANALYSIS

The quasielastic scattering data presented here have been compared to a calculation based on a distorted-wave impulse approximation (DWIA). The DWIA is extensively reviewed in Ref. 3. In the present application, the expression for the differential cross section associated with two observed outgoing nucleons must be integrated over all final momenta of the unobserved struck nucleon. This integration has been performed by Kroll and Wall.[18] With the aid of several approximations, they derive the following expression for the differential cross section corresponding to scattering of the incident proton into solid angle $d\Omega_1$ and energy interval dE_1. (In the present analysis the energy interval dE_1 has been replaced by the momentum interval dp_1.)

TABLE VII. Smoothed cross sections in units of mb/[sr(MeV/c)] for an angle of 25°. These cross sections were obtained by smoothing point by point data obtained in this work. In some cases the interpolation has been performed between nonoverlapping data sets at different momenta.

P (MeV/c)	^{6}Li	Li	^{12}C	^{27}Al	^{40}Ca	^{51}V	^{90}Zr	Pb
970	0.0455	0.051	0.092	0.147				
980	0.0450	0.052	0.092	0.147				
990	0.0445	0.052	0.091	0.148				
1000	0.0440	0.053	0.091	0.149				
1010	0.0455	0.053	0.091	0.151				
1020	0.0460	0.054	0.092	0.154				
1030	0.0470	0.054	0.093	0.156				0.340
1040	0.0480	0.056	0.096	0.161		0.211	0.278	0.341
1050	0.0500	0.057	0.099	0.165		0.216	0.284	0.343
1060	0.0520	0.060	0.103	0.169		0.220	0.285	0.345
1070	0.0540	0.065	0.107	0.174		0.224	0.289	0.348
1080	0.0590	0.072	0.115	0.182	0.208	0.229	0.298	0.353
1090	0.0650	0.077	0.124	0.189	0.228	0.234	0.305	0.360
1100	0.0730	0.083	0.129	0.195	0.231	0.239	0.315	0.368
1110	0.0810	0.091	0.135	0.202	0.240	0.245	0.328	0.380
1120	0.0910	0.100	0.143	0.212	0.252	0.256	0.340	0.390
1130	0.1020	0.113	0.153	0.224	0.268	0.266	0.355	0.408
1140	0.1110	0.123	0.162	0.234	0.278	0.277	0.370	0.428
1150	0.1220	0.134	0.170	0.244	0.290	0.289	0.385	0.448
1160	0.1340	0.146	0.177	0.254	0.303	0.300	0.405	0.470
1170	0.1480	0.158	0.186	0.264	0.315	0.312	0.423	0.495
1180	0.1610	0.168	0.197	0.276	0.330	0.324	0.443	0.528
1190	0.1710	0.176	0.202	0.284	0.341	0.335	0.458	0.558
1200	0.1780	0.181	0.204	0.290	0.354	0.344	0.473	0.595
1210	0.1840	0.186	0.210	0.294	0.364	0.352	0.483	0.620
1220	0.1870	0.186	0.216	0.296	0.368	0.358	0.493	0.638
1230	0.1880	0.184	0.218	0.296	0.374	0.363	0.498	0.651
1240	0.1835	0.178	0.214	0.294	0.364	0.372	0.496	0.654
1250	0.1730	0.170	0.206	0.288	0.360	0.361	0.484	0.653
1260	0.158	0.159	0.196	0.278	0.344	0.353	0.465	0.645
1270	0.140	0.143	0.184	0.268	0.320	0.342	0.449	0.630
1280	0.120	0.119	0.175	0.254	0.310	0.329	0.451	0.600
1290	0.103	0.110	0.162	0.237	0.294	0.309	0.450	0.575
1300	0.091	0.094	0.144	0.230	0.272	0.291	0.410	0.553
1310	0.077	0.075	0.130	0.209	0.253	0.276	0.358	0.523
1320	0.065	0.065	0.115	0.186	0.220	0.240	0.323	0.488
1330	0.053	0.054	0.100	0.160	0.202	0.225	0.310	0.430
1340	0.044	0.045	0.087	0.136	0.170	0.190	0.283	0.385
1350	0.037	0.038	0.074	0.118	0.152	0.171	0.249	0.340
1360	0.031	0.034	0.064	0.102	0.142	0.161	0.223	0.295
1370	0.025	0.028	0.054	0.091	0.120	0.133	0.193	0.263
1380	0.021	0.025	0.051	0.084	0.094	0.118	0.158	0.230
1390	0.020	0.022	0.045	0.065	0.076	0.104	0.125	0.205
1400	0.019	0.019	0.037	0.052	0.068	0.083	0.108	0.184
	±4.8 [a]	±4.8	±4.3	±3.9	±4.3	±3.9	±3.9	±4.3

[a] Approximate systematic cross section errors in %.

$$\frac{d^2\sigma}{d\Omega_1 dE_1} = \frac{1}{(\hbar c)^2} \sum_{\alpha=1}^{A} \frac{4\pi k_1}{k_0 x} \int dk_{A-1} k_{A-1} \frac{m_0^2 + E_0 E_\alpha - p_0 p_\alpha \cos(x, k_\alpha)\cos(x, k_0)}{E_\alpha} \left(\frac{d\sigma}{d\Omega}\right)_{p-N}^{\text{c.m.}} \frac{\sum m_l |g_{njlm_l}(\vec{k}_\alpha)|^2}{2l+1} . \quad (1)$$

In Eq. (1), $\vec{x} = \vec{k}_0 - \vec{k}_1$ and

$$g_{njlm_l}(\vec{k}_\alpha) = \frac{1}{(2\pi)^{3/2}} \int d\vec{r}_\alpha e^{-i\vec{k}_\alpha \cdot \vec{r}_\alpha} D_2^*(\vec{r}_\alpha) D_1^*(\vec{r}_\alpha) D_0(\vec{r}_\alpha) \frac{u_{nlj}(r_\alpha)}{r_\alpha} Y_{lm}(\theta_\alpha, \phi_\alpha) \quad (2)$$

TABLE VIII. Smoothed cross sections in units of mb/[sr(MeV/*c*)] for an angle of 30°. These cross sections were obtained by smoothing point by point data obtained in this work. In some cases the interpolation has been performed between nonoverlapping data sets at different momenta.

P (MeV/*c*)	^{6}Li	Li	^{12}C	^{27}Al	^{40}Ca	^{51}V	^{90}Zr	^{208}Pb
900	0.0355	0.0379	0.076		0.161	0.168	0.251	0.326
910	0.0365	0.0382	0.078		0.162	0.168	0.252	0.324
920	0.0375	0.0388	0.079	0.130	0.162	0.169	0.252	0.322
930	0.0379	0.0396	0.080	0.131	0.163	0.169	0.253	0.321
940	0.0385	0.0402	0.082	0.131	0.164	0.169	0.253	0.320
950	0.0391	0.0414	0.083	0.133	0.166	0.170	0.254	0.317
960	0.0400	0.0426	0.084	0.133	0.167	0.170	0.255	0.318
970	0.0412	0.0447	0.085	0.134	0.168	0.172	0.256	0.318
980	0.0426	0.0471	0.088	0.134	0.169	0.174	0.258	0.321
990	0.0440	0.0497	0.090	0.135	0.170	0.176	0.260	0.323
1000	0.0459	0.0532	0.091	0.136	0.173	0.179	0.261	0.324
1010	0.0473	0.0560	0.092	0.137	0.178	0.180	0.263	0.327
1020	0.0495	0.0592	0.095	0.140	0.181	0.182	0.264	0.331
1030	0.0512	0.0631	0.097	0.144	0.186	0.185	0.265	0.337
1040	0.0542	0.0661	0.099	0.147	0.189	0.188	0.267	0.341
1050	0.0592	0.0702	0.100	0.149	0.193	0.191	0.270	0.346
1060	0.0669	0.0743	0.103	0.154	0.199	0.192	0.272	0.350
1070	0.0737	0.0781	0.105	0.156	0.204	0.195	0.276	0.355
1080	0.0791	0.0817	0.108	0.160	0.207	0.199	0.282	0.367
1090	0.0828	0.0850	0.110	0.162	0.211	0.201	0.286	0.374
1100	0.0858	0.0876	0.111	0.164	0.214	0.205	0.291	0.380
1110	0.0885	0.0897	0.114	0.167	0.218	0.207	0.297	0.388
1120	0.0909	0.0909	0.115	0.169	0.219	0.208	0.300	0.394
1130	0.0922	0.0909	0.116	0.173	0.220	0.207	0.303	0.407
1140	0.0928	0.0903	0.117	0.174	0.218	0.205	0.303	0.414
1150	0.0917	0.0882	0.118	0.174	0.213	0.204	0.303	0.421
1160	0.0844	0.0850	0.117	0.173	0.209	0.201	0.302	0.421
1170	0.0773	0.0808	0.115	0.169	0.206	0.199	0.299	0.420
1180	0.0698	0.0758	0.110	0.164	0.203	0.195	0.294	0.409
1190	0.0627	0.0704	0.103	0.160	0.199	0.193	0.289	0.405
1200	0.0560	0.0651	0.098	0.151	0.190	0.188	0.284	0.398
1210	0.0509	0.0592	0.091	0.143	0.183	0.183	0.277	0.399
1220	0.0468	0.0539	0.088	0.136	0.176	0.177	0.269	0.379
1230	0.0430	0.0483	0.080	0.128	0.166	0.169	0.254	0.359
1240	0.0391	0.0426	0.076	0.121	0.157	0.161	0.244	0.334
1250	0.0361	0.0385	0.071	0.112	0.147	0.153	0.232	0.329
1260	0.0331	0.0408	0.065	0.105	0.136	0.143	0.218	0.320
1270	0.0305	0.0320	0.059	0.097	0.125	0.135	0.206	0.301
1280	0.0284	0.0288	0.053	0.091	0.111	0.121	0.174	0.253
1290	0.0246	0.0258	0.049	0.083	0.102	0.109	0.155	0.238
1300	0.0222	0.0234	0.043	0.074	0.088	0.101	0.148	0.211
1310	0.0195	0.0207	0.038	0.066	0.080	0.088	0.134	0.185
1320	0.0160	0.0187	0.033	0.058	0.071	0.080	0.114	0.173
1330	0.0134	0.0157	0.028	0.048	0.061	0.070	0.103	0.140
1340	0.0110	0.0128	0.025	0.043	0.051	0.056	0.088	0.125
1350	0.0086	0.0110	0.022	0.036	0.043	0.047	0.076	0.112
1360	0.0075	0.0098	0.019	0.030	0.038	0.040	0.064	0.097
1370	0.0080	0.0080	0.017	0.024	0.033	0.034	0.052	0.084
1380	0.0057	0.0053	0.012	0.018	0.021	0.027	0.043	0.058
1390	0.0033	0.0027	0.008	0.014	0.016	0.019	0.036	0.050
1400	0.0021	0.0024	0.006	0.009	0.013	0.015	0.027	0.038
	±5.4 [a]	±5.4	±5.0	±4.6	±5.0	±4.6	±4.6	±5.0

[a] Approximate systematic cross sections errors in %.

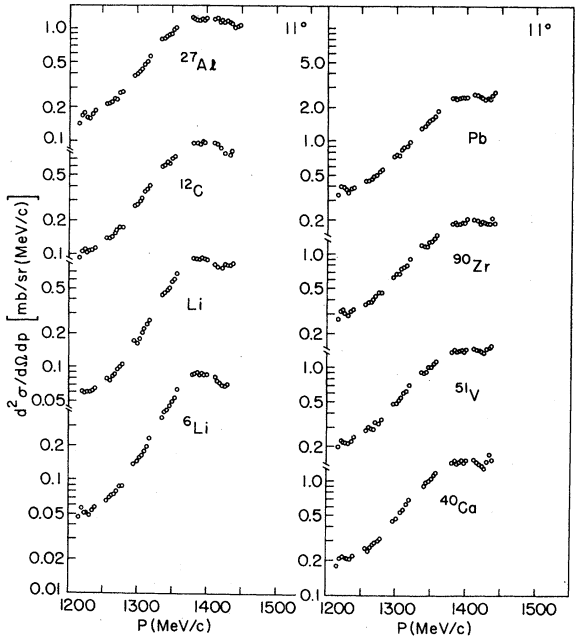

FIG. 6. Proton spectra for eight targets over the quasifree region at a laboratory scattering angle of 11°. The curves are eye guides.

The subscripts 0, α, 1, and 2 refer to the incident proton, the struck nucleon, the observed proton and the unobserved nucleon, respectively. The residual recoiling nucleus is labeled "$A-1$." The differential cross section $(d\sigma/d\Omega)^{\text{c.m.}}_{p-N}$ refers to the

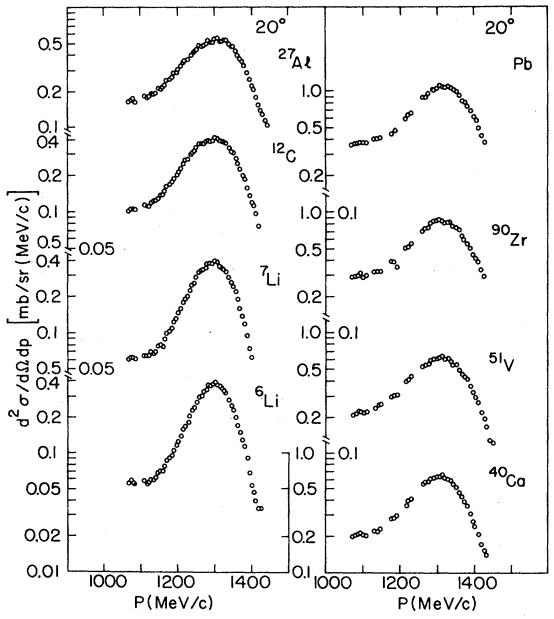

FIG. 7. Proton spectra for eight targets over the quasifree region at a laboratory scattering angle of 20°. The curves are eye guides.

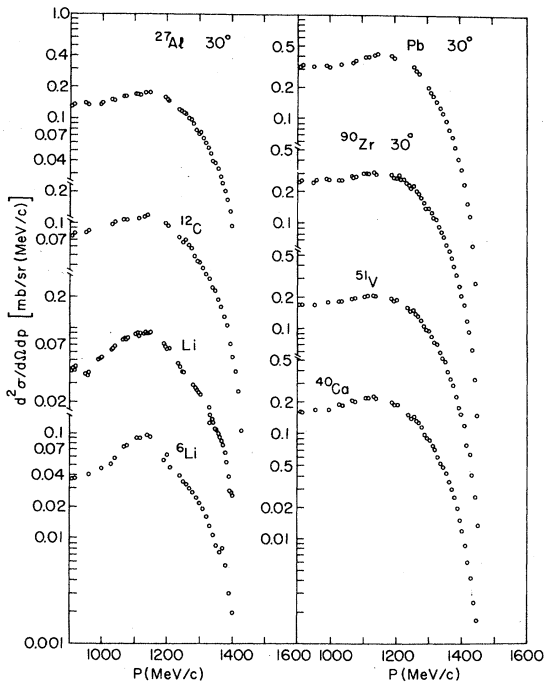

FIG. 8. Proton spectra for eight targets over the quasifree region at a laboratory scattering angle of 30°. The curves are eye guides.

free $p-N$ cross section in the c.m. system corresponding to the $p-N$ collision specified by the laboratory momenta $\vec{k}_0$, $\vec{k}_\alpha$, $\vec{k}_1$, and $\vec{k}_2$. (In Ref. 18 the $p-N$ differential cross section is taken to be the $p-p$ differential cross section.) The D's are the distortion factors while the u's are the optical model bound state wave functions. Further details concerning the notation in Eqs. (1) and (2) can be found in Ref. 18. In these equations $g(\vec{k})$ is called the "distorted momentum distribution." It differs from the actual distribution, obtained from a Fourier transform of the bound state wave function, by the presence of the distortion factors D_i. These serve to modify the momentum of the target nucleon in the nucleon-nucleon collision to account for the effect of multiple collisions on the incoming and outgoing projectile nucleon (refraction and absorption).

The bound state wave functions $u_{nlj}(r_\alpha)$ of the struck nucleons have been calculated with the A-THREE optical model program,[19] using parameters found in the literature.[3,20,21] Binding energies not available in the literature were obtained by searching in A-THREE using predetermined well depths. To simplify the calculations proton optical model wave functions were used for all target nucleons (whether neutrons or protons) in filled shells, while for the unfilled shells, neutron wave functions were generally used. It is emphasized,

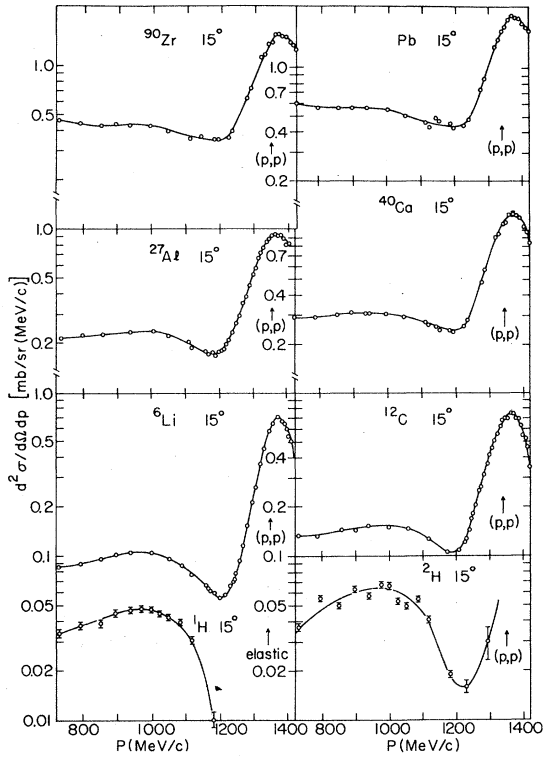

FIG. 9. Proton spectra for the delta isobar and quasielastic regions at a laboratory scattering angle of 15°. The curves are eye guides.

however, that in the calculation of Eq. (1), the proper distinction between struck neutrons and protons has been made in evaluating the elementary differential cross section $(d\sigma/d\Omega)p-N$, as has already been mentioned above.

The distortion factors $D_i(\vec{r})$ $(i=0,1,2)$ are evaluated using a distorted high-energy optical model square-well potential V_i+iW_i, as discussed in Ref. 18. Solving a one-dimensional Schrödinger equation with this potential and with a WKB approximation, one obtains[18,22]

$$D_i(\vec{r})=\exp\{[-iE_i/(\hbar c)^2k_i][V_i+iW_i]\Delta S\}\,, \quad i=0,1,2 \qquad (3)$$

where ΔS is the path length of the particle i in the nuclear medium. Since, in the present experiment particle 2 is unobserved, we set $V_2=W_2=0$, following the argument in Ref. 18. Moreover, it has been found that the calculated cross sections are very insensitive to the values of V_0 and V_1, which have therefore been set to equal 0.

As might be expected, the calculated cross sections are found to be very sensitive to W_0 and W_1, since these lead to attenuation of the incoming and outgoing waves. We have chosen to let $W_0=W_1$

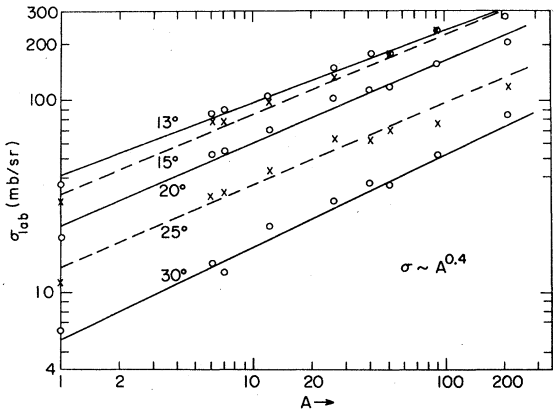

FIG. 10. The integrated cross section under the quasielastic peak as a function of mass number. Data from successive angles are marked alternatively ○ and ×. Hydrogen elastic scattering is plotted at $A=1$.

and to regard W_0 as a fitting parameter. More precisely, we have determined W_0 by fitting the calculated peak value of the spectrum at $\theta=13°$ to the peak of the 13° experimental data. This value of W_0 is then used for the calculation of the spectra at the other angles (20° and 30°). The values of W_0 so obtained are listed in Table IX.

From Eq. (3) it can be seen that the mean free path l for absorption of protons in the nucleus can be related to the value of W_0 by means of

$$l=(\hbar c)^2k/2E|W_0|\,. \qquad (4)$$

If we take $|W_0|=24$ MeV, which is the average value of $|W_0|$ as determined from Table I, and $E=1738$ MeV, $k=7.415$ fm^{-1}, we find $l=3.46$ fm. On the other hand, the value of l can also be found from the relation

$$l=\frac{1}{n\sigma_a}\,, \qquad (5)$$

where n, the density of nucleons, is roughly 0.14 fm^{-3} and σ_a, the cross section for removal of the incident proton from the quasielastic peak, i.e., the cross section for meson production, is roughly 1.7 fm^2.[16] We find therefore

$$l=4.20 \text{ fm}\,,$$

which is in fair agreement with the value obtained in (4).

We conclude that these values for W_0, shown in Table IX, are in qualitative agreement with what is expected from general physical arguments.

A computer code to evaluate Eqs. (1) and (2) had been developed by Kroll[22] and applied by him to ^{12}C and ^{40}Ca quasielastic scattering. We have substantially modified this code in the following ways.

(1) An empirical energy- and isospin-dependent

TABLE IX. The values for W_0, the absorptive potential, required to fit the peak values for the quasielastic region in the DWIA analysis of the data.

Target	$-W_0$(MeV)
^{6}Li	17
^{7}Li	10
^{12}C	26
^{27}Al	27
^{40}Ca	26
^{51}V	24
^{90}Zr	20.5
^{208}Pb	37

elementary proton-nucleon differential cross section $(d\sigma/d\Omega)^{\text{c.m.}}_{p-N}$ has been inserted. The elementary proton-nucleon differential cross section is parametrized following the analysis and data contained in the review article of Alkhazov *et al.*[23] The cross section contains contributions from both central (C) and spin-orbit (S) amplitudes

$$\frac{d\sigma}{d\Omega} = |f^C(q)|^2 + |f^S(q)|^2 , \tag{6}$$

where q is the momentum transfer and a cross term has been eliminated by averaging over spins. The central amplitude is written as

$$f^C(q) = f^C(0)e^{-\beta^2 q^2/2} , \tag{7}$$

$f^C(0)$ being the forward scattering amplitude and β^2 the "shape parameter." To find the imaginary part of $f^C(0)$ the optical theorem is used, i.e., since $f^S(0) = 0$,

$$\mathrm{Im}[f^C(0)] = \frac{k\sigma_{\text{total}}}{4\pi} , \tag{8}$$

where σ_{tot} is the total cross section at momentum k. The total cross section is found from a parametrization due to Harp.[24] Combining (7) and (8) we get

$$f^C(q) = \left(\frac{k\sigma_{\text{tot}}}{4\pi}\right)(\epsilon + i)\exp(-\beta^2 q^2/2) , \tag{9}$$

where ϵ is the ratio of the real to the imaginary part of the $f^C(q)$. The spin-orbit amplitude is parametrized by analogy with (9):

$$f^S(q) = \gamma\left(\frac{k\sigma_{\text{tot}}}{4\pi}\right)(\epsilon_S + i)q\exp(-\beta_S{}^2 q^2/2) . \tag{10}$$

Equations (6), (9), and (10) are now used to calculate the differential cross section. The values of the parameters in these expressions are as follows.

In the case of $p-p$ cross section, we have, from the data of Alkhazov *et al.*, the empirical relation

$$\epsilon_{pp} = 0.7505 - 4.72\times 10^{-4} p_{0L} , \tag{11}$$

where p_{0L} is the laboratory momentum of the incident particle expressed in MeV/c.

For $\beta_{pp}{}^2$ we find

$$\beta_{pp}{}^2 = 11.6(\log_{10} p_{0L} - 2.751) . \tag{12}$$

For the $p-n$ cross section we find

$$\epsilon_{pn} = 0.7184 - 7.184\times 10^{-4} p_{0L} \tag{13}$$

and

$$\beta_{pn}{}^2 = 9.439(\log_{10} p_{0L} - 26.157) . \tag{14}$$

For both $p-n$ and $p-p$

$$\gamma = 0.16 \text{ fm}, \quad \epsilon_S = -0.1, \quad \beta_S{}^2 = 0.66 \text{ fm}^2 .$$

(2) The algorithm for the calculation of the distortion factors $D_i(\vec{r})$ has been altered to take the distortion into account when the struck nucleon is outside the nominal nuclear radius. Let R denote the radius of the target nucleus as used in the bound state calculation and let r, θ, ϕ denote the spherical coordinates of the struck nucleon, the polar axis being along the direction of the incident beam.

If $r \leq R$, Kroll's algorithm is followed. If $r > R$, whereas Kroll's algorithm would yield no distortion, the new version of the code first compares the impact parameter $r\sin\theta$, to R. If $r\sin\theta \geq R$, there is no distortion, but if $r\sin\theta < R$, the total path length is assumed to be the average chord length through a sphere of radius R, i.e., $\frac{4}{3}R$, with $\frac{2}{3}R$ traversed before collision and $\frac{2}{3}R$ traversed after collision. These path lengths are then inserted into the expressions for the distortion factors as given by Eq. (3).

(3) The code has been extended to include nuclei heavier than ^{12}C.

(4) The need for a Fourier transform of the bound state wave function as input to the code has been eliminated. The above modifications have substantially improved the agreement between the data and predictions of the program. Calculations with the modified DWIA code have been performed for scattering angles of 13°, 20°, and 30° and for all the target nuclei used in the experiment and have been compared with the data. Examples of these fits are discussed in the next section.

V. CONCLUSIONS AND SUMMARY

We illustrate the application of the DWIA analysis for several of the targets and the scattering angles measured. Some typical comparisons are shown in Figs. 11–13. These figures display two features of the DWIA analysis which seem to be characteristic for all the targets considered.

(1) The DWIA analysis tends to produce a quasielastic peak which is narrower than the data,

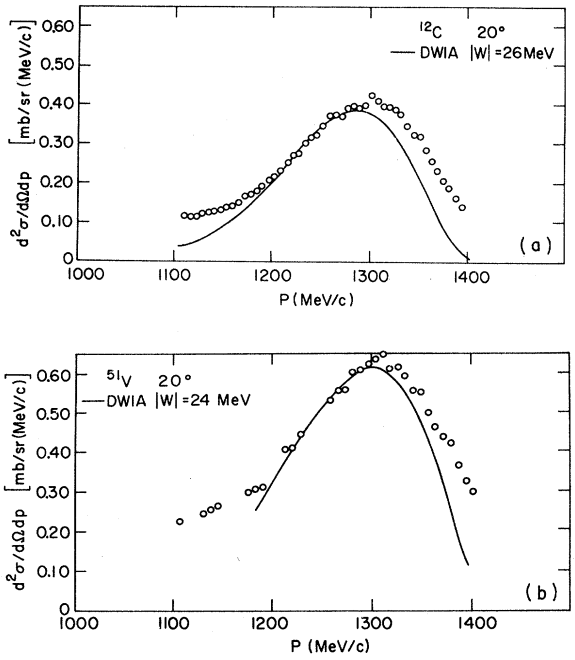

FIG. 11. (a) Experimental results for ^{12}C at 20° compared to a DWIA calculation using an absorptive potential of 26 MeV. (b) Experimental results for ^{51}V at 20° compared to a DWIA calculation using an absorptive potential of 24 MeV.

especially at laboratory angles larger than 20°.

(2) The DWIA analysis predicts a peak momentum which is consistently below that of the data. In fact the centroids of the observed nuclear quasifree peaks are (within the experimental uncertainty, typically ±1 MeV/c) identical to that for the free ^{1}H $(p,p)^1$H elastic scattering process. The shift predicted by the DWIA results simply from the binding of the nucleon within the nuclear well. The ^{51}V and ^{12}C fits are obtained by setting $W_0 = W_1 = 24$ to 26 MeV, and $V_0 = V_1 = 0$. The values for $W_{0,1}$ were obtained by adjusting the calculation to produce the observed peak cross section at 13°. For most nuclides investigated, reasonable agreement between experiment and calculation for values near $W_0 = 24$ MeV can be obtained, in the sense that the cross sections near the quasielastic peak are reproduced.

The experimental data also tend to show structure at the positions expected for nucleon scattering from mass 2 or mass 4 clusters. These structures are most pronounced, however, for ^{6}Li and ^{9}Be and are the subject of a continuing investigation which will be reported elsewhere.

While the problem of matching width and position persists at all angles, there are systematic aspects to the discrepancy which can be illustrated by several examples. In Figs. 12 and 13 are shown

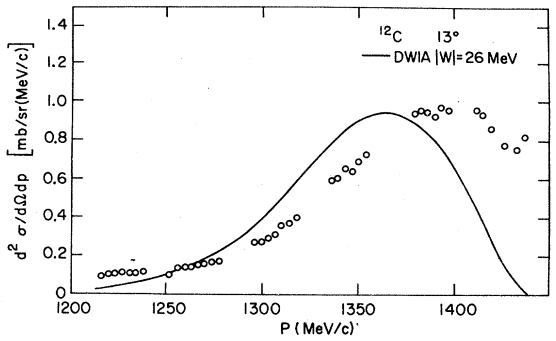

FIG. 12. Experimental results for ^{12}C at 13° compared to a DWIA calculation using an absorptive potential of 26 MeV.

DWIA curves for ^{12}C at 13° and for ^{90}Zr at 30°. For the 13° ^{12}C data, the agreement is excellent provided one translates the DWIA curve by 20 MeV/c from what is shown in the figure.

At 30°, as shown for ^{90}Zr, the peak position is apparently given well by DWIA; here, however, the width of this peak attributed to quasifree scattering is significantly narrower than the observed distribution. The width deficiency is even more emphatic for a heavier nucleus such as ^{208}Pb.

These general trends are observable for all nuclides and are possibly due to the gross approximation inherent in our use of the Kroll and Wall version of the DWIA calculation. One essential feature of that calculation is the treatment of the struck nucleon: It is assumed to escape from the nucleus and its binding energy is included in the kinematic calculations. At small scattering angles, however, the momentum transferred to the struck nucleon is small enough that its escape from the nucleus is far from probable. The WKB approximation of Eq. (3) is not valid for very small values of k_i. We have avoided this problem by not distorting the struck or unobserved particle. A proper quantum mechanical treatment,

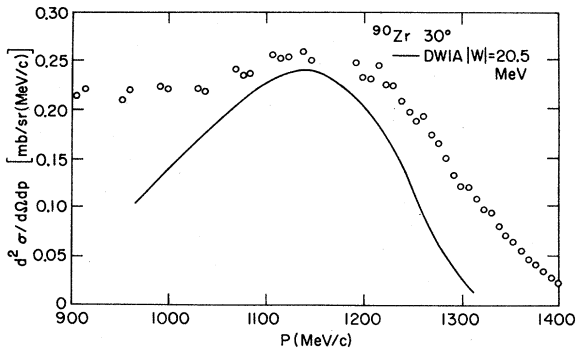

FIG. 13. Experimental results for ^{90}Zr at 30° compared to a DWIA calculation using an absorptive potential of 20.5 MeV.

however, must include this distortion and we conclude that the shift in peak position produced by the calculation is attributable to our neglect of the distortion for this particle. Thus at small scattering angles (<20°) in the laboratory frame a significant component of the scattering cross section in the neighborhood of the quasielastic peak corresponds to coherent inelastic scattering events to highly excited states in the residual target nucleus. A phenomenological way to treat the shift is to introduce an "effective" binding energy E_b' $< E_b$, into the calculation. The first order effect of such an E_b' is just to shift the calculated peak position. Agreement in position may be obtained with an effective binding energy of a few MeV. At laboratory scattering angles larger than 15°, the escape of the struck nucleon is virtually certain and the DWIA calculation is a good representation of the data.

At angles larger than 20°, and particularly for heavy nuclei, the observed proton will have a significant probability for undergoing several collisions, so that a single scattering at an angle θ may be simulated by a number of small angle scatterings. The DWIA calculation, which is a single scattering approximation, can fail badly. Abul-Magd and Guardiola[25] have shown that double scattering effects are small at small angles, but are increasingly important at angles corresponding to large momentum transfers. The quasielastic peak is therefore considerably spread by the effect of these multiple scatterings. Only near 20° is the straightforward DWIA calculation capable of accurately reproducing the data.

The imaginary part of the optical model potential used in the DWIA distortion factors yields a value for the nuclear mean free path for absorption which is in satisfactory agreement with the nucleon density and the pion production cross sections.

ACKNOWLEDGMENTS

The authors wish to acknowledge the assistance of the operating staff of the LAMPF HRS, particularly the invaluable help of Gerry Hoffman in mounting and running the experiment. We are also indebted to G. Blanpied, M. Oouthoudt, and Roger Liljestrand for assistance in taking the data. The assistance of Mrs. Jean Domish, Reinhard Schumacher, and David DeMarco in carrying out the analysis is also gratefully acknowledged. N. S. Wall of the University of Maryland was extremely helpful in providing Kroll's DWIA code and advice and encouragement. Research has been performed under contracts EY-76-C-02-0016 and EG-77-S-02-4195 with the U. S. Department of Energy.

[1]R. Serber, Phys. Rev. 72, 1114 (1947).
[2]M. L. Goldberger, Phys. Rev. 74, 1269 (1948).
[3]R. Bengtsson, T. Berggren, and Ch. Gustafson, Phys. Rep. 41, 191 (1978) and references contained therein.
[4]R. M. Sternheimer and S. J. Lindenbaum, Phys. Rev. 105, 1874 (1951).
[5]D. M. Corley, N. S. Wall, H. Palevsky, J. L. Friedes, R. J. Sutter, G. W. Bennett, W. D. Simpson, G. C. Phillips, G. J. Igo, and R. L. Stearns, Nucl. Phys. A184, 437 (1972).
[6]J. W. Wachter, W. A. Gibson, and W. R. Burrus, Phys. Rev. C 6, 1496 (1972).
[7]N. S. Wall and P. R. Roos, Phys. Rev. 150, 811 (1966).
[8]L. S. Azghirey, I. K. Vzorov, V. P. Zrelov, M. C. Mescheryakov, B. S. Neganov, R. M. Ryndin, and A. F. Shabudin, Nucl. Phys. 13, 258 (1959).
[9]K. Strauch and F. Titus, Phys. Rev. 104, 191 (1956).
[10]J. B. Cladis, W. N. Hess, and B. J. Moyer, Phys. Rev. 87, 425 (1952).
[11]P. A. Wolff, Phys. Rev. 87, 434 (1952).
[12]H. Tyrén, Th. A. J. Maris, and P. Hillman, Nuovo Cimento 6, 1507 (1957); H. Tyrén, P. Hillman, and Th. A. J. Maris, Nucl. Phys. 7, 10 (1958).
[13]G. Blanpied, Los Alamos Scientific Laboratory Report No. LA-7262T, 1978, pp. 8-27 (unpublished).
[14]H. B. Willard, B. D. Anderson, H. W. Baer, R. J. Barrett, P. R. Bevington, A. N. Anderson, H. Wilmes, and N. Jarmie, Phys. Rev. C 14, 1545 (1976).
[15]G. D. Harp, K. Chen, G. Friedlander, Z. Frankel, and J. M. Miller, Phys. Rev. C 8, 581 (1973).
[16]G. D. Harp, Phys. Rev. C 10, 2387 (1974).
[17]K. Chen, Z. Fraenkel, G. Friedlander, J. R. Grover, J. M. Miller, and Y. Shimamoto, Phys. Rev. 166, 949 (1968).
[18]F. R. Kroll and N. S. Wall, Phys. Rev. C 1, 138 (1970).
[19]E. H. Auerbach, Comput. Phys. Commun. 15, 165 (1978).
[20]L. R. B. Elton and A. Swift, Nucl. Phys. A94, 52 (1967).
[21]A. H. Wapstra, At. Data Nucl. Data Tables 19, 175 (1977).
[22]F. R. Kroll, Thesis, University of Maryland, 1968 (unpublished).
[23]G. D. Alkhazov, S. L. Belostotsky, and A. A. Vorobyov, Phys. Rep. 42C, 89 (1978).
[24]G. D. Harp, private communication.
[25]A. Y. Abul-Magd and R. Guardiola, Nuovo Cimento 8A, 108 (1972).